
Adaptive Bayesian Multivariate Spline Knot Inference with Prior Specifications on Model Complexity

Junhui He

Department of Mathematical Sciences
Tsinghua University
Beijing, China
hejh22@mails.tsinghua.edu.cn

Ying Yang

Department of Mathematical Sciences
Tsinghua University
Beijing, China
yangying@tsinghua.edu.cn

Jian Kang

Department of Biostatistics
University of Michigan, Ann Arbor
Michigan, United States
jiankang@umich.edu

Abstract

In multivariate spline regression, the number and locations of knots influence the performance and interpretability significantly. However, due to non-differentiability and varying dimensions, there is no desirable frequentist method to make inference on knots. In this article, we propose a fully Bayesian approach for knot inference in multivariate spline regression. The existing Bayesian method often uses BIC to calculate the posterior, but BIC is too liberal and it will heavily overestimate the knot number when the candidate model space is large. We specify a new prior on the knot number to take into account the complexity of the model space and derive an analytic formula in the normal model. In the non-normal cases, we utilize the extended Bayesian information criterion to approximate the posterior density. The samples are simulated in the space with differing dimensions via reversible jump Markov chain Monte Carlo. We apply the proposed method in knot inference and manifold denoising. Experiments demonstrate the splendid capability of the algorithm, especially in function fitting with jumping discontinuity.

1 Introduction

Spline regression [Wahba, 1990, Schumaker, 2007, Gu, 2013] is a nonparametric method for modelling the complex dependencies between features, widely used in many fields including machine learning, econometrics and biomedicine. It is an ideal alternative to linear regression in the nonlinear data analysis. However, given the number and location of knots, the spline space is actually a linear space with a spline basis. Thus, the spline regression degenerates to a simple linear regression with respect to the basis, posing a strict limitation on its representative capacity. The ordinary solution is to assign sufficiently many knots and locate them uniformly, leading to a trade-off between the complexity and the flexibility of splines; see smoothing splines and thin plate splines [Wood, 2003]. Furthermore, the splines with fixed knots usually assume each knot is used only once. This means the spline function has continuous derivatives up to its degree minus one. Consequently, it is inappropriate for the distinct-knot spline to fit curves with jumping discontinuity.

Rather than equally-spaced knots, we develop a Bayesian approach for the automatic selection of the spline knots. The basic principle is modelling the intricate relationships with a few knots and the optimal location. The adaptive knot method reduces the complexity of splines when preserving the

flexibility. We can also model the sharp changes by placing several knots in the almost coincident position. Moreover, the knot estimation provides a mechanism for easy interpretation. The number of knots detects how many transitions occur and the location indicates where change points lie. Thus, the quantities are of independent interest in many applications. For example, by examining the approval ratings of successful politicians, the president can determine the optimal time to switch from the job of governing to the job of running for reelection [Marsh and Cormier, 2001]. See Aminikhanghahi and Cook [2017], Truong et al. [2020] for a review about the change point detection in time series.

A considerable amount of work has been done for the knot selection. Some researchers rely on specialist knowledge or exploratory data analysis to specify the knots heuristically. But the ad hoc manner is rough since the exact knot information is unknown. Lerman [1980] chose the knots via a grid-search method, whose search time grows exponentially with the increasing sample size. Muggeo [2003] proposed a segmented regression method to estimate the break-point location based on a linearization technique and developed an R package [Muggeo, 2008]. But this method is limited to linear splines and the number of knots is required to be known. For likelihood-based inference, the primary difficulty is that the likelihood is not differentiable with respect to the knots. Given the number of knots, Ritabrata Das and Zheng [2016] utilized local quadratic smoothing to approximate linear spline models and Guangyu Yang and Zhang [2023] proposed modified derivatives of the likelihood at the knots. However, the knot number cannot be estimated in the two methods.

Bayesian approaches were also proposed in the literature. Denison et al. [1998b] proposed an automatic Bayesian curve fitting method and extended it to multivariate splines in Denison et al. [1998a]. However, they did not derive the correct dimensional penalty factor and the method involved hyperparameter determination. Dimatteo et al. [2001] developed a Bayesian adaptive regression spline method for the knot estimation. They employed the Bayesian information criterion (BIC) to calculate the marginal likelihood and simulated samples via reversible jump Markov chain Monte Carlo (RJMCMC) of Green [1995]. However, the prior of the knot number doesn't take into account the complexity of the model space when the parametric dimension changes, and BIC seems to be too liberal as evaluation criteria when the number of all possible knots is large. Besides, this method is restricted to univariate splines. Fearnhead [2006] proposed a recursive approach to calculate the density and performed direct simulation from the posterior distribution. But the computational complexity is quadratic in the sample size, making it a slow method. Refer to Chen et al. [2011] for a detailed comparison about the Bayesian knot estimation.

In this article, we will propose an extended Bayesian adaptive regression spline (EBARS) method for estimating the number and location of multivariate spline knots simultaneously. The tensor product spline [Dierckx, 1995] is used to make predictions in the multiple regression case. We consider the complexity of the model space and thereby assign a specific prior on the number of knots to adjust the effect. We specify a unit information prior [Kass and Wasserman, 1995] for the spline coefficients. An analytic expression of the evidence is derived in the normal noise model. For the non-normal cases, we utilize the extended Bayesian information criterion (EBIC) for the approximation. Similar to Dimatteo et al. [2001], the posterior simulation is performed via RJMCMC. We compare the performance with several methods in knot inference through extensive simulations. Experiments demonstrate the excellent performance of our method in scenarios with single or multiple knots, with or without jumping discontinuity. Furthermore, we develop a manifold estimation technique as an application of the proposed method. An R package is available in the GitHub repository <https://github.com/junhuihe2000/EBARS>.

The paper is organized as follows: Section 2 presents the detailed Bayesian spline knot selection method; Section 3 describes the sampling procedure of RJMCMC; Section 4 evaluates the proposed algorithm in knot inference and manifold denoising through numerical experiments; Section 5 concludes and discusses the future research.

2 Extended Bayesian adaptive regression spline

We are considering the tensor product spline for modeling the dependencies between a single response variable and multiple predictor variables. Generally, the number and locations of knots determine the smoothness of splines and affect the performance substantially. Our objective is to select optimal nodes by a Bayesian approach.

Assume labeled observations $\{(x_i, y_i)\}_{i=1}^m \subset [0, 1]^d \times \mathbb{R}$ are independent and identically distributed, such that for $i = 1, \dots, m$,

$$y_i = f(x_i) + \epsilon_i, \quad \epsilon_i \sim N(0, \sigma^2), \quad (1)$$

where $f : [0, 1]^d \rightarrow \mathbb{R}$ is an unknown function, and $\sigma^2 > 0$ is the noise variance.

2.1 Tensor product spline regression model

The article utilizes tensor product splines to model the real multivariate function f . As the name implies, the tensor product spline space is the tensor product of d univariate spline spaces corresponding to each component of x . The univariate spline space in $[0, 1]$ of degree p_i and non-decreasing knot sequence $\{\xi_{ij}\}_{j=0}^{k_i+1}$ allowing duplicates ($\xi_{i0} = 0, \xi_{i(k_i+1)} = 1$) consists of the following univariate functions: (1) Be a polynomial of at most degree p_i on each interval $(\xi_{ij}, \xi_{i(j+1)})$; (2) Belong to $C^{p_i-1}([0, 1])$ except for the coincident knots, and if $\xi_{i(j-1)} < \xi_{ij} = \dots = \xi_{i(j+l)} < \xi_{i(j+l+1)}$, the function has continuous derivatives up to the order $p_i - 1 - l$ at that point ($l \leq p_i$). Specifically, when $l = p_i$, the spline function may discontinue at the coincident knot.

Remark 1. *The usual spline-based methods employ equidistant knots or quantile-based knots, posing the distinct knot assumption implicitly. This results in continuous splines. When the true function exists jumping discontinuity, the distinct knot spline will fail to make an accurate estimation. However, the spline with automatic knot selection can circumvent the problem by optimal placement.*

Let $p = \{p_i\}_{i=1}^d$, $k = \{k_i\}_{i=1}^d$, and $\xi = \{\xi_i\}_{i=1}^d$ with $\xi_i = \{\xi_{ij}\}_{j=1}^{k_i}$. Denote the tensor product spline space as $\mathcal{S}_{p,k,\xi}$ and the univariate spline space as $\mathcal{S}_{p_i,k_i,\xi_i}$ for $i = 1, \dots, d$. Then $\mathcal{S}_{p,k,\xi} = \bigotimes_{i=1}^d \mathcal{S}_{p_i,k_i,\xi_i}$, where $\mathcal{S}_{p_i,k_i,\xi_i}$ is a linear space with the dimension of $k_i + p_i + 1$. Let $\{b_{ij}\}_{j=1}^{k_i+p_i+1}$ be a basis of $\mathcal{S}_{p_i,k_i,\xi_i}$, such as B-splines. Consequently, the dimension of $\mathcal{S}_{p,k,\xi}$ is $\prod_{i=1}^d (k_i + p_i + 1)$, denoted as ν . And $b = \bigotimes_{i=1}^d \{b_{ij}\}_{j=1}^{k_i+p_i+1}$ is a basis of $\mathcal{S}_{p,k,\xi}$. For simplicity, rewrite b as $\{b_i\}_{i=1}^\nu$. Thus, any $f \in \mathcal{S}_{p,k,\xi}$ can be represented by $\sum_{i=1}^\nu \beta_i b_i$. Let $\beta = (\beta_1, \dots, \beta_\nu)^\top$. Define the design matrix Z by $Z_{ij} = b_j(x_i)$ for $i = 1, \dots, m$ and $j = 1, \dots, \nu$. Therefore, (1) can be reformulated as

$$y = Z\beta + \epsilon, \quad \epsilon \sim N_m(0, \sigma^2 I_m), \quad (2)$$

where $y, \epsilon \in \mathbb{R}^m$, $\beta \in \mathbb{R}^\nu$, $Z \in \mathbb{R}^{m \times \nu}$. Notably, (2) is an ordinary linear regression model.

2.2 Prior & posterior

Experiments have demonstrated that changes on p have little impact on the performance; see Perperoglou et al. [2019]. Cubic splines ($p = 3$) and linear splines ($p = 1$) are the most common alternatives in the research. We will explore the two splines in the simulations. Given the degree, the number and position of knots determine basis functions of the spline space, affecting the non-linearity in the model.

We specify the priors of k, ξ, β, σ in (2) as follows. Firstly, we initialize enormous candidate knots. Owing to the specific structure of tensor product splines, the candidate knots can be chosen in each component separately. Let n_i nodes $\eta_i \subset [0, 1]$ be the i -th component. Then the overall candidate knots are given by $\eta = \bigotimes_{i=1}^d \eta_i$. To simplify the analysis, assume that the knots in η_i are distinct. Nevertheless, when n_i is sufficiently large and η_i is sufficiently dense in $[0, 1]$, we can still find a spline model to reflect jumping discontinuity well. For $i = 1, \dots, d$, let \mathcal{M}_{k_i} be the model space containing all the possible location combinations with k_i knots in $[0, 1]$. Then the size of \mathcal{M}_{k_i} is $\tau(\mathcal{M}_{k_i}) = \binom{n_i}{k_i}$. Since $k_i \ll n_i$, $\tau(\mathcal{M}_{k_i})$ is increasing as k_i increases. Let \mathcal{M}_k be $\bigotimes_{i=1}^d \mathcal{M}_{k_i}$. Then $\tau(\mathcal{M}_k) = \prod_{i=1}^d \binom{n_i}{k_i}$. The priors of k, ξ are specified as

$$\pi(k) \propto \tau(\mathcal{M}_k)^{1-\gamma}, \quad \pi(\xi|k) = 1/\tau(\mathcal{M}_k), \quad 0 \leq \gamma \leq 1. \quad (3)$$

Consequently, $\pi(k, \xi) \propto \tau(\mathcal{M}_k)^{-\gamma}$. Given k , the prior probabilities of different position combinations are equal. The parameter γ adjusts the growth rate of $\pi(k)$. It is equivalent to imposing a penalty on $\pi(k)$. As γ increases from 0 to 1, the growth rate becomes milder gradually. Particularly, when $\gamma = 0$, we have $\pi(k) \propto \tau(\mathcal{M}_k)$ and $\pi(k, \xi) \propto 1$, meaning the same prior probability for knots. Sometimes this γ causes that excessive knots are selected.

Suppose $k_1, \dots, k_d \ll m$, then $Z^\top Z$ is of full rank. In terms of β, σ , we assume

$$\beta|Z, \sigma \sim N_\nu(0, m\sigma^2(Z^\top Z)^{-1}), \quad \pi(\sigma) = 1/\sigma, \quad \sigma > 0. \quad (4)$$

The prior of β is the so-called unit information prior. According to the linear regression theory, the least squares estimator of β is $\hat{\beta} = (Z^\top Z)^{-1}Z^\top y$. Then the precision matrix (inverse covariance) is given by $(Z^\top Z)/\sigma^2$. The unit precision matrix is defined as $(Z^\top Z)/m\sigma^2$, implying the prior of β in (4). The prior of σ is an improper prior as $\int_0^\infty 1/\sigma d\sigma = \infty$.

According to the Bayesian formula, the posterior density of k, ξ, β, σ is

$$p(k, \xi, \beta, \sigma|y) = p(\beta, \sigma|k, \xi, y)p(k, \xi|y), \quad (5)$$

where $p(k, \xi|y) \propto p(y|k, \xi)\pi(k, \xi)$. Let $a_{k, \xi} = y^\top(I_m - \frac{m}{m+1}Z(Z^\top Z)^{-1}Z^\top)y$.

Lemma 1. *With the above priors of k, ξ, β, σ in (2), we have*

$$p(y|k, \xi) \propto (m+1)^{-\nu/2} a_{k, \xi}^{-m/2}, \quad p(k, \xi|y) \propto (m+1)^{-\nu/2} a_{k, \xi}^{-m/2} \tau(\mathcal{M}_k)^{-\gamma}. \quad (6)$$

The posterior $p(k, \xi|y)$ consists of three main components. The first term $(m+1)^{-\nu/2}$ serves as the dimensional penalty. It balances the number of parameters and the bias of model fitting. The second term $a_{k, \xi}^{-m/2}$ represents the effect of the likelihood. When m is sufficiently large, $a_{k, \xi}$ is approximately equal to the residual sum of squares. The third term $\tau(\mathcal{M}_k)^{-\gamma}$ corresponds to the priors of k, ξ . It takes the complexity of \mathcal{M}_k into consideration.

Subsequently, we can simulate samples of β, σ given k, ξ from the conditional posterior density in (5) via a Gibbs sampler, contributing to a fully Bayesian model.

2.3 Extended Bayesian information criterion

The Gaussian prior of β is a conjugate prior in (2), yielding a closed expression of $p(y|k, \xi)$. Generally, $p(y|k, \xi)$ is analytically intractable except for the normal regression model. For those non-conjugate cases, we utilize the extended Bayesian information criterion (EBIC) of Chen and Chen [2008] to approximate the posterior density. In the spline knot estimation, the cardinality of all candidate knots (*i.e.*, n) can be very large but the number of the true knots (*i.e.*, k) is small compared to the sample size (*i.e.*, m). Thus, EBIC will be extremely useful for model selection as the small- m -large- n assumption holds and the Laplace approximation is valid [Foygel and Drton, 2010, Chen and Chen, 2012, Luo et al., 2015].

According to the definition, the EBIC of k, ξ is

$$\text{BIC}_\gamma(k, \xi) = -2 \log L(\hat{\beta}, \hat{\sigma}|y, k, \xi) + (\nu+1) \log m + 2\gamma \log \tau(\mathcal{M}_k), \quad 0 \leq \gamma \leq 1, \quad (7)$$

where $\hat{\beta}, \hat{\sigma}$ are the maximum likelihood estimators of β, σ given k, ξ . Especially in (2), $\hat{\beta} = (Z^\top Z)^{-1}Z^\top y$ and $\hat{\sigma}^2 = y^\top(I_m - Z(Z^\top Z)^{-1}Z^\top)y/m$. As $\gamma = 0$, (7) is the ordinary BIC. Since $n_1, \dots, n_d \gg m$, the EBIC with $\gamma > 0$ is preferable to the ordinary BIC in knot estimation. From the Laplace approximation, $p(k, \xi|y) \approx \exp\{-\text{BIC}_\gamma(k, \xi)/2\}$, denoted by $\hat{p}(k, \xi|y)$.

Lemma 2. *In multivariate spline model (2), the EBIC approximation of the posterior density is*

$$\hat{p}(k, \xi|y) \propto m^{-(\nu+1)/2} (\hat{\sigma}^2)^{-m/2} \tau(\mathcal{M}_k)^{-\gamma}. \quad (8)$$

Suppose k', ξ' are another group of knots. Comparing (6) and (8), we can find $p(k, \xi|y)/p(k', \xi'|y) \approx \hat{p}(k, \xi|y)/\hat{p}(k', \xi'|y)$ when m is sufficiently large. Since the sampling procedure of MCMC is determined by the posterior density ratio, the EBIC contributes to a consistent estimation.

3 Reversible jump Markov chain Monte Carlo

The reversible jump approach [Green, 1995] is an extension of the standard Metropolis-Hastings algorithm, allowing the trans-dimensional movement. These algorithms are widely used in the (Bayesian) model determination problems where the dimension of parameters is unknown [Bolton and Heard, 2018, Chapple et al., 2020].

In this section we use RJMCMC to obtain samples of k, ξ from the posterior distribution (6) or (8). Due to the tensor product structure, the sampling procedure can be performed in the component individually. Suppose x_i is the current update component. When modifying x_i , other components are invariant. We design three transition strategies to traverse the state space: (1) Birth: add a knot with the probability $b_{k_i} = c \min(1, \{(n_i - k_i)/(k_i + 1)\}^{1-\gamma})$; (2) Death: delete a knot with the probability $d_{k_i} = c \min(1, \{k_i/(n_i - k_i + 1)\}^{1-\gamma})$; (3) Relocation: change the position of one knot with the probability $r_{k_i} = 1 - b_{k_i} - d_{k_i}$. The hyper-parameter c is of the interval $(0, 0.5)$. Notably, $\pi(k_i)b_{k_i} = \pi(k_i + 1)d_{k_i+1}$, satisfying the detailed balance equation for the prior of the knot number. Suppose the jumping probability is $q(k'_i, \xi'_i | k_i, \xi_i)$. Let $\xi_{i,k_i} \subset \eta_i$ be the locations of k_i knots in the i -th component. The concrete proposal distributions are specified in the following manner:

1. *Birth step.* Select a knot from the remaining candidate knots $\eta_i \setminus \xi_{i,k_i}$ uniformly, and add it into ξ_{i,k_i} . Then $q(k_i + 1, \xi_{i,k_i+1} | k_i, \xi_{i,k_i}) = b_{k_i}/(n_i - k_i)$.
2. *Death step.* Select a knot from the current knots ξ_{i,k_i} uniformly, and delete it. Then $q(k_i - 1, \xi_{i,k_i-1} | k_i, \xi_{i,k_i}) = d_{k_i}/k_i$.
3. *Relocation step.* Select a knot from ξ_{i,k_i} and another knot from $\eta_i \setminus \xi_{i,k_i}$ uniformly. Exchange their positions. Then $q(k_i, \xi'_{i,k_i} | k_i, \xi_{i,k_i}) = r_{k_i}/\{k_i(n_i - k_i)\}$.

Assume that (k, ξ) is the current status and (k', ξ') is the candidate status. To sample from the target posterior distribution, the Metropolis-Hastings algorithm implies that,

$$p(k, \xi | y) q(k', \xi' | k, \xi) \alpha(k', \xi' | k, \xi) = p(k', \xi' | y) q(k, \xi | k', \xi') \alpha(k, \xi | k', \xi'), \quad (9)$$

where $\alpha(k', \xi' | k, \xi)$, $\alpha(k, \xi | k', \xi')$ are the acceptance probabilities.

Lemma 3. *With the specified proposal distribution and the posterior density of (9), the acceptance probability and its EBIC approximation in RJMCMC are*

$$\begin{aligned} \alpha(k', \xi' | k, \xi) &= \min\{1, (m+1)^{(\nu-\nu')/2} (a_{k,\xi}/a_{k',\xi'})^{m/2}\}, \\ \hat{\alpha}(k', \xi' | k, \xi) &= \min\{1, m^{(\nu-\nu')/2} (\hat{\sigma}^2/(\hat{\sigma}')^2)^{m/2}\}, \end{aligned} \quad (10)$$

where ν, ν' are the dimensions of the spline space.

Lemma 3 implies that $\sqrt{m+1}$, \sqrt{m} are the dimensional penalty factors for the likelihood. Comparing $\alpha(k', \xi' | k, \xi)$ and $\hat{\alpha}(k', \xi' | k, \xi)$ in (10), $\alpha \approx \hat{\alpha}$ when the sample size is sufficiently large. The overall extended Bayesian adaptive regression spline approach is listed as Algorithm 1.

Algorithm 1 Extended Bayesian adaptive regression spline algorithm via RJMCMC

Input: Labeled observations $\{(x_i, y_i)\}_{i=1}^m$, hyper-parameters $0 \leq \gamma \leq 1$ and $0 < c < 0.5$, jumping steps I , the number of candidate knots n .

- 1: Create the candidate knots η . Initialize the starting knots $(k^{(0)}, \xi^{(0)})$.
- 2: **for** $i = 0, \dots, I - 1$ **do**
- 3: Determine the j -th component to update randomly and choose the transition strategy.
- 4: Solve (k', ξ') for the next movement by the proposal distribution.
- 5: Compute $\alpha(k', \xi' | k^{(i)}, \xi^{(i)})$ by (10). Sample $u \sim U(0, 1)$.
- 6: **if** $u < \alpha(k', \xi' | k^{(i)}, \xi^{(i)})$ **then**
- 7: Update the knots by $(k^{(i+1)}, \xi^{(i+1)}) = (k', \xi')$;
- 8: **else**
- 9: Return to Step 3 and repeat.
- 10: **end if**
- 11: **end for**

Output: The posterior samples $\{k^{(i)}, \xi^{(i)}\}_{i=1}^I$.

4 Experiment

We conduct EBARS in the knot inference and manifold denoising. For the knot inference, the performance is compared with the segmented method of Muggeo [2003] and the modified maximum likelihood (MML) method of Guangyu Yang and Zhang [2023]. For the manifold denoising, the

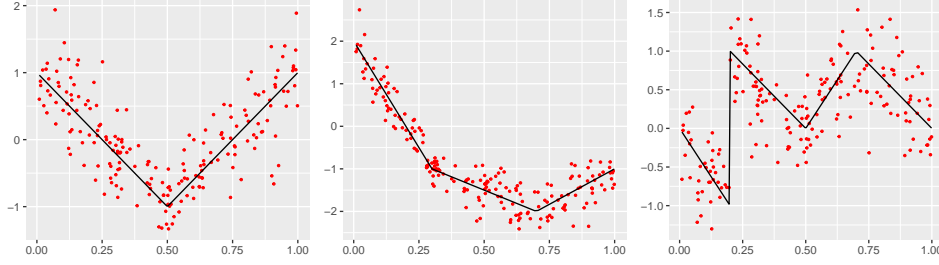


Figure 1: Linear splines with one, two and four knots. Black segments are true spline curves and red points are noisy observed data with $m = 200$.

Table 1: Absolute errors for knot location estimation of three methods in $k = 1, 2$

Methods	m	One knot	Two knots	
		Knot 1	Knot 1	Knot 2
EBARS	200	0.0219(0.0126)	0.0167(0.0150)	0.0248(0.0257)
MML		0.0163(0.0099)	0.0138(0.0118)	0.0170(0.0214)
Segmented		0.0159(0.0102)	0.0117(0.0113)	0.0186(0.0204)
EBARS	500	0.0100(0.0076)	0.0095(0.0065)	0.0142(0.0122)
MML		0.0075(0.0060)	0.0068(0.0058)	0.0102(0.0076)
Segmented		0.0079(0.0061)	0.0070(0.0059)	0.0113(0.0081)

performance is compared with manifold fitting under unbounded noise (MFUN) of Yao and Xia [2023], putative manifold fitting (PMF) of Fefferman et al. [2018], principal manifold estimation (PME) of Meng and Eloyan [2021] and principal curves (PC) of Hastie and Stuetzle [1989]. Numerical experiments show that the proposed method performs well in finite samples of all scenarios.

4.1 Knot inference

We perform EBARS for knot inference in linear spline regression. Line segments are connected in unique knots and the spline is discontinuous at the location where two knots coincide. The data is generated from three linear spline models with one, two and four knots as shown in Figure 1, where the knot locations are respectively (0.5) , $(0.3, 0.7)$, $(0.2, 0.2, 0.5, 0.7)$. The functions are continuous except for the spline with $k = 4$. The noise is Gaussian with standard deviation 0.4, 0.3, 0.4.

Figure 2 illustrates the posterior distribution of the knot number and location by EBARS with $\gamma = 1$ in $k = 1, 2, 4$. The sample size is 500 in all scenarios. We simulate 5000 samples of (k, ξ) via RJMCMC after 5000 burning steps. Histograms show that the average knot number is close to the true value with negligible error. From the density plots, the posterior mass concentrates on the correct location of change points in all cases even though the knot number is unknown. Especially, for $k = 4$, the posterior density at 0.2 is double at 0.5 and 0.7, meaning that 0.2 is chosen as the knot twice.

To evaluate the performance of knot inference, we compare EBARS with Segmented of Muggeo and MML of Guangyu Yang and Zhang. In this experiment, the knot number is given since Segmented and MML cannot estimate k . The absolute error of knot location is calculated as criteria. Three methods are evaluated under sample sizes $m = 200, 500$ and the experiment is repeated 50 times.

Simulation results of the mean and standard deviation of absolute errors are summarized in Tables 1 and 2. When $k = 1, 2$, three methods obtain fairly small absolute errors. However, when $k = 4$, the absolute errors of EBARS are much less than other two algorithms for all knots. MML struggles to estimate the duplicate knots 0.2 and causes horrible bias. Segmented outperforms MML but it is still much less accurate than EBARS. Compared with MML and Segmented, our EBARS is robust and attain a precise estimation with jumping discontinuity and increasing number of knots. Furthermore, MML and Segmented are exclusively applied in linear splines and they require the knot number to be given, whereas EBARS is convenient to estimate the knot number and location simultaneously in splines of any degree.

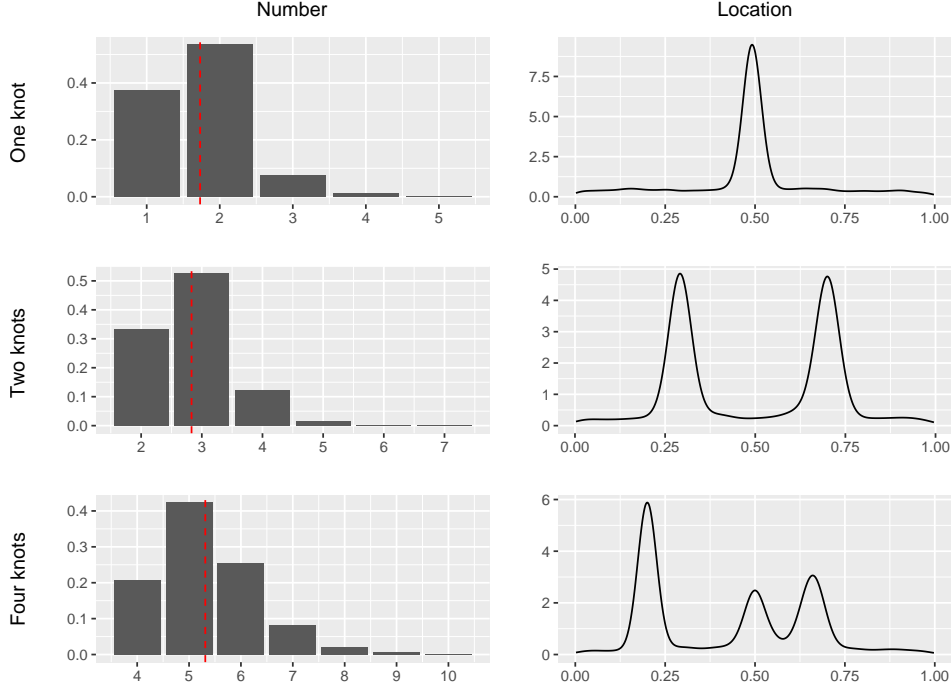


Figure 2: The posterior distributions of knots in three scenarios by EBARS. Left channels are the histograms of the knot number, where red dashed vertical lines indicate the mean number. Right channels are the posterior density plots of the knot location.

Table 2: Absolute errors for knot location estimation of three methods in $k = 4$

Methods	m	Four knots			
		Knot 1	Knot 2	Knot 3	Knot 4
EBARS	200	0.0058(0.0060)	0.0044(0.0043)	0.0206(0.0199)	0.0170(0.0096)
MML		0.3437(1.1010)	0.1163(0.1283)	0.0978(0.1006)	0.1012(0.1454)
Segmented		0.0366(0.0494)	0.0712(0.1067)	0.0799(0.0889)	0.0752(0.0805)
EBARS	500	0.0025(0.0029)	0.0026(0.0025)	0.0194(0.0172)	0.0150(0.0137)
MML		0.2737(0.4266)	0.1725(0.1683)	0.1065(0.1800)	0.2131(0.5211)
Segmented		0.0171(0.0346)	0.0283(0.0775)	0.0395(0.0825)	0.0349(0.0805)

4.2 Manifold denoising

With the assumption of linearity, principal component analysis is a prevailing and efficient method for dimension reduction in high-dimensional space. However, the simple method poses a limitation to respect the nonlinear relationship. Manifold estimation is a technique for modelling the complicated dependence in high-dimensional data, denoising the observations and estimating the low-dimensional latent manifold. Refer to Yao et al. [2024] for a detailed review about manifold estimation.

Assume that the observed data $\{x_i\}_{i=1}^m$ is generated from a low-dimensional latent manifold of a high-dimensional ambient space with random noise. That is,

$$X = W + \epsilon, \quad X, \epsilon \in \mathbb{R}^D, \quad W \in \mathbb{M}^d,$$

where \mathbb{M}^d is a d -dimensional submanifold of \mathbb{R}^D with $d \leq D$, W is generated from a probability distribution supported in \mathbb{M}^d , and ϵ is D -dimensional noise independent of W . In this article, we propose a two stage manifold estimation (TSME) technique for modelling \mathbb{M}^d . The primary challenge of parametrization is attributed to the lack of the required pairs of training data, *i.e.*, (predictor, response). We resolve the issue simply by combining the manifold embedding and reconstruction. The manifold embedding is a nonlinear dimensional reduction method. Many impressive algorithms

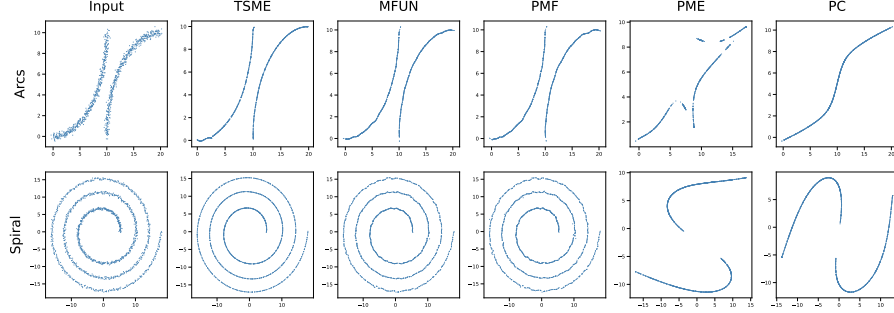


Figure 3: Manifold denoise results for two curve scenarios. Each plot indicates the training samples or the denoised representation obtained by our TSME, MFUN, PMF, PME and PC.

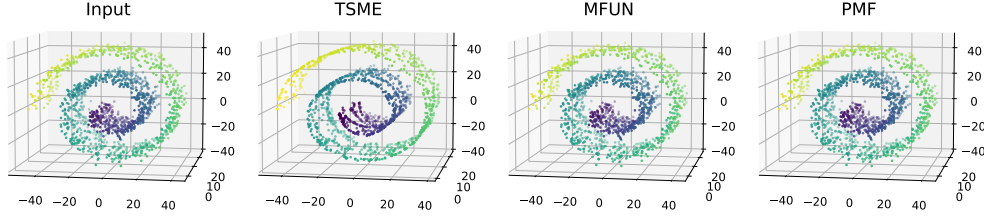


Figure 4: Manifold denoise results for the Swiss roll. Each plot indicates the training samples or the denoised representation obtained by our TSME, MFUN and PMF.

have been proposed in the literature, such as ISOMAP [Balasubramanian and Schwartz, 2002], Laplacian eigenmaps [Belkin and Niyogi, 2003] and UMAP [McInnes et al., 2020].

At the first stage, we apply the manifold embedding technique in $\{x_i\}_{i=1}^m$ given the intrinsic dimension d , yielding a projection map $\hat{g} : \mathbb{R}^D \rightarrow \mathbb{R}^d$. Let $u_i = \hat{g}(x_i)$ for $i = 1, \dots, m$. Then $\{(u_i, x_i)\}_{i=1}^m$ are the training samples for the manifold reconstruction. At the second stage, we execute the regression in $\{(u_i, x_i)\}_{i=1}^m$ to reconstruct the manifold. For example, we can use the proposed EBARS method to estimate the reconstruction map \hat{f} . Due to the automatic knot selection, EBARS is eligible to model the complex relationships between u and x . Consequently, the manifold estimation is completed by the composition of the embedding \hat{g} and the reconstruction \hat{f} . Especially, $\{\hat{f} \circ \hat{g}(x_i)\}_{i=1}^m$ can serve as the denoised representation of $\{x_i\}_{i=1}^m$.

We conduct the TSME method in manifold denoising and compare its performance with MFUN, PMF, PME and PC. Notably, PME and PC adopt a similar framework with our TSME except that they utilize smoothing splines for reconstruction. The data is generated from two disconnected arcs in \mathbb{R}^2 , a spiral curve in \mathbb{R}^2 and a Swiss roll in \mathbb{R}^3 , as shown in Figures 3 and 4. ISOMAP is used as the embedding map of TSME and the initial projection of PME in the spiral and Swiss roll. For the arc case, we substitute UMAP for ISOMAP due to the disconnectivity. Besides, for the Swiss roll, we only compare TSME, MFUN and PMF, as PC is limited to the curve case and PME is very slow with disastrous performance. The random noise is Gaussian with standard deviation 0.2, 0.2, 1.5.

Simulation results including the training samples and the denoised data are visualized in Figures 3 and 4. The sample sizes are $m = 1000, 1500, 3000$. Compared with TSME, the PME and PC methods collapse dramatically in curve cases. In arcs, the disconnectivity of \mathbb{M}^d causes the jumping discontinuity of the reconstruction map. In spiral, the dependency is complex due to the intricate manifold, posing a critical challenge in selecting the optimal penalty weight of smoothing splines. For MFUN and PMF, the denoised representations remain corrupted in the spiral and Swiss roll cases. They don't mitigate the random noise successfully and fail to estimate the latent manifolds accurately.

Table 3: Summary of GMSD with respect to five methods in three manifolds

	Arcs	Spiral	Swiss roll
m	500	1000	1500
Input	0.0404(0.0020)	0.0397(0.0021)	2.6033(0.0729)
TSME	0.0036(0.0021)	0.0019(0.0003)	0.5299(0.0653)
MFUN	0.0039(0.0011)	0.0112(0.0011)	2.5549(0.0735)
PMF	0.0051(0.0011)	0.0165(0.0017)	2.5994(0.0733)
PME	0.4790(0.2585)	2618.6(9887.4)	×
PC	0.7661(0.0077)	2.9539(0.0633)	×
m	1000	1500	3000
Input	0.0399(0.0013)	0.0401(0.0013)	2.6423(0.0621)
TSME	0.0044(0.0033)	0.0015(0.0002)	0.5004(0.0605)
MFUN	0.0018(0.0004)	0.0078(0.0005)	2.5377(0.0629)
PMF	0.0023(0.0007)	0.0113(0.0008)	2.6241(0.0625)
PME	0.3135(0.1353)	151.87(449.52)	×
PC	0.7589(0.0072)	2.9601(0.0699)	×

To evaluate the performance quantitatively, we define the geometric mean squared distance as

$$\text{GMSD} = \frac{1}{m} \sum_{i=1}^m \text{dist}(\hat{f} \circ \hat{g}(x_i), \mathbb{M}^d)^2,$$

where $\text{dist}(x, \mathbb{M}^d) = \inf_{x' \in \mathbb{M}^d} \|x - x'\|$. The GMSD measures the corrupted extent of the data away from the manifold. Table 3 illustrates the mean and standard deviation of GMSD in three manifolds of 20 duplicates. TSME obtains significantly smaller GMSD than the training samples in all scenarios and achieves the smallest GMSD in most cases, demonstrating that our method contributes to excellent manifold denoising. For MFUN and PMF, the performance in the $d = 1$ cases is satisfactory but the noise is not reduced in the Swiss roll. PME and PC are completely incapable of estimating the latent manifolds.

5 Conclusion

This article is motivated by the knot selection problem in the multivariate spline regression. The proposed method estimates the number and location of spline knots simultaneously and accurately. It provides a mechanism for easy interpretation and function fitting with jumping discontinuity. The trade-off for advantages is the additional computational cost, attributed to RJMCMC. Nevertheless, it will not cause a serious problem in small or moderately large datasets.

There are several potential jobs in the future. We intend to establish a theoretical framework of the algorithm including the consistency and convergence rate. The primary challenge is how to define an appropriate distance between parameters with varying dimensions. Furthermore, the domain space is required to be a cube. We aim for an extension in the general domain. A possible solution is substituting a flexible multivariate spline for the tensor product spline.

6 Code and technical appendices

The source package EBARS is accessible on the GitHub repository <https://github.com/junhuihe2000/EBARS> and R codes of examples in Section 4 are available on the GitHub repository <https://github.com/junhuihe2000/exampleEBARS>. The technical appendices include proofs of Lemmas 1 and 3, and additional simulations in curve and surface fitting.

Acknowledgements

Yang’s research was partially supported by the National Natural Science Foundation of China grant (12271286, 11931001). Kang’s research was partially supported by the following grants: NIH R01DA048993, NIH R01MH105561 and NSF IIS2123777.

References

- S. Aminikhanghahi and D. J. Cook. A survey of methods for time series change point detection. *Knowledge and Information Systems*, 51(2):339–367, 2017.
- M. Balasubramanian and E. L. Schwartz. The isomap algorithm and topological stability. *Science*, 295(5552):7–7, 2002.
- M. Belkin and P. Niyogi. Laplacian eigenmaps for dimensionality reduction and data representation. *Neural Computation*, 15(6):1373–1396, 2003.
- A. D. Bolton and N. A. Heard. Malware family discovery using reversible jump MCMC sampling of regimes. *Journal of the American Statistical Association*, 113(524):1490–1502, 2018.
- A. G. Chapple, T. Peak, and A. Hemal. A novel Bayesian continuous piecewise linear log-hazard model, with estimation and inference via reversible jump Markov chain Monte Carlo. *Statistics in Medicine*, 39(12):1766–1780, 2020.
- C. W. Chen, J. S. Chan, R. Gerlach, and W. Y. Hsieh. A comparison of estimators for regression models with change points. *Statistics and Computing*, 21:395–414, 2011.
- J. Chen and Z. Chen. Extended Bayesian information criteria for model selection with large model spaces. *Biometrika*, 95(3):759–771, 09 2008.
- J. Chen and Z. Chen. Extended BIC for small-n-large-p sparse GLM. *Statistica Sinica*, 22(2): 555–574, 2012.
- D. G. T. Denison, B. K. Mallick, and A. F. M. Smith. Bayesian MARS. *Statistics and Computing*, 8: 337–346, 1998a.
- D. G. T. Denison, B. K. Mallick, and A. F. M. Smith. Automatic Bayesian curve fitting. *Journal of the Royal Statistical Society: Series B (Statistical Methodology)*, 60(2):333–350, 1998b.
- P. Dierckx. *Curve and Surface Fitting with Splines*. Oxford University Press, New York, 1995.
- I. Dimatteo, C. R. Genovese, and R. E. Kass. Bayesian curve-fitting with free-knot splines. *Biometrika*, 88(4):1055–1071, 12 2001. ISSN 0006-3444.
- P. Fearnhead. Exact and efficient Bayesian inference for multiple changepoint problems. *Statistics and Computing*, 16:203–213, 2006.
- C. Fefferman, S. Ivanov, Y. Korylev, M. Lassas, and H. Narayanan. Fitting a putative manifold to noisy data. In S. Bubeck, V. Perchet, and P. Rigollet, editors, *Proceedings of the 31st Conference On Learning Theory*, volume 75, pages 688–720. PMLR, 06–09 Jul 2018.
- R. Foygel and M. Drton. Extended Bayesian information criteria for Gaussian graphical models. *Advances in Neural Information Processing Systems*, 23, 2010.
- P. J. Green. Reversible jump Markov chain Monte Carlo computation and Bayesian model determination. *Biometrika*, 82(4):711–732, 12 1995.
- P. J. Green and B. W. Silverman. *Nonparametric Regression and Generalized Linear Models: A Roughness Penalty Approach*. Chapman and Hall, London, 1994.
- C. Gu. *Smoother Spline ANOVA Models*. Springer, New York, 2013.
- B. Z. Guangyu Yang and M. Zhang. Estimation of knots in linear spline models. *Journal of the American Statistical Association*, 118(541):639–650, 2023.
- T. Hastie and W. Stuetzle. Principal curves. *Journal of the American Statistical Association*, 84(406): 502–516, 1989.
- R. E. Kass and L. Wasserman. A reference Bayesian test for nested hypotheses and its relationship to the Schwarz criterion. *Journal of the American Statistical Association*, 90(431):928–934, 1995.

- P. M. Lerman. Fitting segmented regression models by grid search. *Journal of the Royal Statistical Society Series C: Applied Statistics*, 29(1):77–84, 3 1980.
- S. Luo, J. Xu, and Z. Chen. Extended Bayesian information criterion in the Cox model with a high-dimensional feature space. *Annals of the Institute of Statistical Mathematics*, 67:287–311, 2015.
- L. C. Marsh and D. R. Cormier. *Spline regression models*. Sage, Iowa, 2001.
- L. McInnes, J. Healy, and J. Melville. UMAP: Uniform manifold approximation and projection for dimension reduction. *Preprint arXiv:1802.03426*, 2020.
- K. Meng and A. Eloyan. Principal manifold estimation via model complexity selection. *Journal of the Royal Statistical Society Series B: Statistical Methodology*, 83(2):369–394, 03 2021.
- V. M. Muggeo. Estimating regression models with unknown break-points. *Statistics in Medicine*, 22(19):3055–3071, 2003.
- V. M. Muggeo. Segmented: an R package to fit regression models with broken-line relationships. *R news*, 8(1):20–25, 2008.
- A. Perperoglou, W. Sauerbrei, M. Abrahamowicz, and M. Schmid. A review of spline function procedures in R. *BMC Medical Research Methodology*, 19:1–16, 2019.
- B. N. Ritabrata Das, Moulinath Banerjee and H. Zheng. Fast estimation of regression parameters in a broken-stick model for longitudinal data. *Journal of the American Statistical Association*, 111(515):1132–1143, 2016.
- L. Schumaker. *Spline Functions: Basic Theory*. Cambridge University Press, New York, 2007.
- C. Truong, L. Oudre, and N. Vayatis. Selective review of offline change point detection methods. *Signal Processing*, 167:107299, 2020.
- G. Wahba. *Spline Models for Observational Data*. Society for Industrial and Applied Mathematics, Philadelphia, 1990.
- S. N. Wood. Thin Plate Regression Splines. *Journal of the Royal Statistical Society Series B: Statistical Methodology*, 65(1):95–114, 2003.
- Z. Yao and Y. Xia. Manifold fitting under unbounded noise. *Preprint arXiv:1909.10228*, 2023.
- Z. Yao, J. Su, and S.-T. Yau. Manifold fitting with cyclegan. *Proceedings of the National Academy of Sciences*, 121(5):e2311436121, 2024. doi: 10.1073/pnas.2311436121.

A Proofs

A.1 Proof of Lemma 1

Proof of Lemma 1. The marginal likelihood $p(y|k, \xi)$ is given by

$$p(y|k, \xi) = p(y|Z) = \int_{(0, \infty)} \int_{\mathbb{R}^\nu} p(y|Z, \beta, \sigma) \pi(\beta|Z, \sigma) \pi(\sigma) d\beta d\sigma.$$

According to the specified priors, we have

$$\begin{aligned} p(y|Z, \beta, \sigma) &= \frac{1}{(2\pi\sigma^2)^{m/2}} \exp\left\{-\frac{1}{2\sigma^2}(y - Z\beta)^\top (y - Z\beta)\right\}, \\ \pi(\beta|Z, \sigma) &= \frac{1}{(2\pi m\sigma^2)^{\nu/2}} |Z^\top Z|^{1/2} \exp\left\{-\frac{1}{2m\sigma^2} \beta^\top Z^\top Z \beta\right\}. \end{aligned}$$

Then the Fubini Thm implies that,

$$p(y|k, \xi) = \int_0^\infty \frac{1}{(2\pi\sigma^2)^{m/2} (m+1)^{\nu/2}} \exp\left\{-\frac{1}{2\sigma^2} a_{k, \xi}\right\} \pi(\sigma) d\sigma,$$

where $a_{k, \xi} = y^\top (I_m - \frac{m}{m+1} Z(Z^\top Z)^{-1} Z^\top) y$. With change of variables $w = \sigma/\sqrt{a_{k, \xi}}$, we have $p(y|k, \xi) \propto (m+1)^{-\nu/2} a_{k, \xi}^{-m/2}$. It follows from $\pi(k, \xi) \propto \tau(\mathcal{M}_k)^{-\gamma}$ that $p(k, \xi|y) \propto (m+1)^{-\nu/2} a_{k, \xi}^{-m/2} \tau(\mathcal{M}_k)^{-\gamma}$. \square

A.2 Proof of Lemma 3

Proof of Lemma 3. According to (9),

$$\alpha(k', \xi'|k, \xi) = \min \left\{ 1, \frac{p(k', \xi'|y) q(k, \xi|k', \xi')}{p(k, \xi|y) q(k', \xi'|k, \xi)} \right\}.$$

Notably, $\pi(k, \xi) q(k', \xi'|k, \xi) = \pi(k', \xi') q(k, \xi|k', \xi')$ under the priors and proposals. Then we have $\alpha(k', \xi'|k, \xi) = \min\{1, p(y|k', \xi')/p(y|k, \xi)\}$. Thus (6) implies this lemma. For the EBIC approximation, we substitute \hat{p} for the corresponding p . \square

B Additional simulation

We conduct EBARS in the curve spline regression ($d = 1, p = 3$) and the surface spline regression ($d = 2, p = 3$). The performance is compared with BARS of Dimatteo et al. [2001], smoothing splines (SS) of Green and Silverman [1994] and thin plate splines (TPS) of Wood [2003]. We calculate the predictive mean squared errors (MSE) for evaluation. Simulations show that the proposed method contributes to accurate predictions of all scenarios.

B.1 Curve spline regression

The curves and data samples involved are illustrated in the first column of Figure 5. It can be seen that data are generated from 4 different smoothness functions, denoted as Cases 1.1 – 1.4 respectively. Cases 1.1 and 1.2 are continuous, whereas Cases 1.3 and 1.4 are discontinuous with one or multiple breakpoints. The outcome noise is Gaussian with standard deviation 2, 2, 4, 1. We compare the prediction performance with BARS and SS in curve fitting. To demonstrate the effect of γ in EBIC, we implement 3 versions of EBARS with $\gamma = 1, 0.5, 0$. All methods are evaluated under sample sizes $m = 200, 500$ and the experiment is repeated 50 times in each setting.

The mean squared errors are summarized in Table 4. To remove the effect of outliers, we drop out points with errors in the top or bottom 2.5% to calculate censored MSE on test data. In EBARS, low γ causes the model overfitting problem. It is clear that MSE rises up gradually as γ decreases, especially in Case 1.3. The behaviour is visualized in columns 2 – 4 of Figure 5. This phenomenon is consistent with the theory. According to EBIC, the prior probability of the model space with k knots satisfies $\pi(\mathcal{M}_k) \propto \tau(\mathcal{M}_k)^{1-\gamma}$. As $k \ll n$ in practice, $\tau(\mathcal{M}_k)$ will grow with increasing number

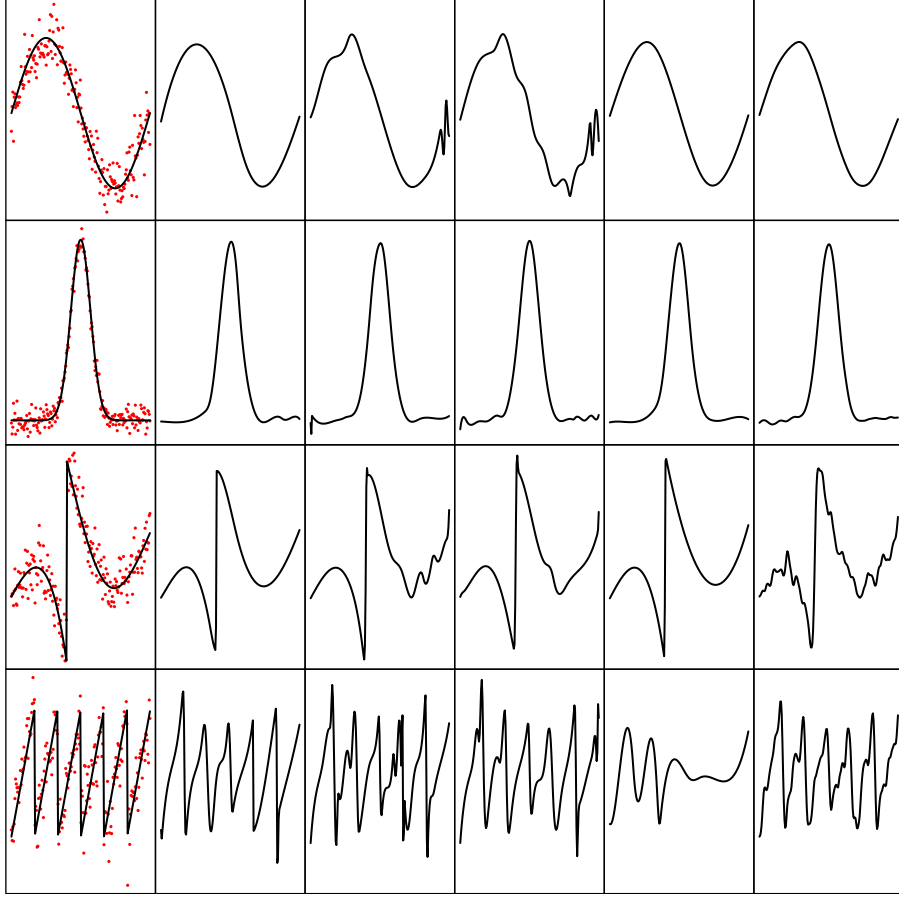


Figure 5: Curve spline regression. It corresponds to the prediction results with $m = 200$ in Cases 1.1 – 1.4. From left to right, columns are respectively the ground truth with red observed points, prediction by EBARS with $\gamma = 1, 0.5, 0$, prediction by BARS and prediction by smoothing splines.

of knots. Consequently, the lower γ means the higher $\pi(\mathcal{M}_k)$ for large k . Thereby more knots will be selected into the model, leading to overfitting in the end.

In this example, $\gamma = 1$ gives the best performance among EBARS. Furthermore, BARS achieves similar results to EBARS $\gamma = 1$ if the true knot number is relatively small, illustrated as in Cases 1.1 – 1.3. However, when the required knot number is really large, BARS fails to work completely and attains a terrible MSE. See the (4, 5) panel of Figure 5 for a graphical explanation. Besides, the smoothing spline method has a severe overfitting problem in Case 1.3, as shown in the (3, 6) panel of Figure 5. This indicates that splines with many misplaced knots are inferior to adaptive knot splines in discontinuous cases.

B.2 Surface spline regression

We compare the performance with BARS and TPS in the surface fitting. The data is generated from four surfaces, denoted as Cases 2.1-2.4. Specifically, Cases 2.1 and 2.2 are smooth, whereas Cases 2.3 and 2.4 are discontinuous. Besides, Case 2.3 is with one jumping point in x_1 and Case 2.4 is with two jumping points in x_1 and x_2 separately. The outcome noise is Gaussian with standard deviation 1, 1.5, 2, 2. To remove outliers in discontinuous cases, we calculate MSE on test data without the upper or lower 2.5% error. All methods are evaluated under sample sizes $m = 500, 1000$ and each experiment is repeated 20 times.

The mean squared errors are summarized in Table 5. Three EBARS versions with $\gamma = 1, 0.5, 0$ are implemented to demonstrate the effect of γ . In Cases 2.1 and 2.2, the performance of all five

Table 4: MSE on test data of five methods in Cases 1.1 – 1.4

Methods	m	Case 1.1	Case 1.2	Case 1.3	Case 1.4
EBARS $\gamma = 1$	200	0.181(0.124)	0.332(0.118)	0.828(0.529)	0.370(0.366)
EBARS $\gamma = 0.5$		0.230(0.136)	0.389(0.184)	1.412(0.783)	0.368(0.150)
EBARS $\gamma = 0$		0.341(0.229)	0.464(0.201)	1.960(0.985)	0.418(0.155)
BARS		0.178(0.150)	0.368(0.139)	0.731(0.403)	3.003(0.504)
SS		0.137(0.088)	0.329(0.132)	3.772(1.687)	0.443(0.155)
EBARS $\gamma = 1$	500	0.068(0.033)	0.147(0.061)	0.361(0.168)	0.079(0.033)
EBARS $\gamma = 0.5$		0.082(0.039)	0.156(0.059)	0.536(0.215)	0.112(0.034)
EBARS $\gamma = 0$		0.170(0.073)	0.231(0.083)	1.053(0.410)	0.144(0.042)
BARS		0.071(0.032)	0.160(0.054)	0.317(0.140)	0.364(0.615)
SS		0.053(0.026)	0.139(0.041)	1.914(0.418)	0.229(0.066)

Table 5: MSE on test data of five methods in Cases 2.1 – 2.4

Methods	m	Case 2.1	Case 2.2	Case 2.3	Case 2.4
EBARS $\gamma = 1$	500	0.163(0.044)	0.624(0.107)	0.664(0.216)	1.133(0.443)
EBARS $\gamma = 0.5$		0.148(0.038)	0.616(0.111)	0.597(0.192)	1.101(0.287)
EBARS $\gamma = 0$		0.138(0.042)	0.609(0.089)	0.568(0.136)	1.076(0.269)
BARS		0.169(0.050)	0.671(0.160)	0.660(0.199)	1.968(0.485)
TPS		0.102(0.031)	0.587(0.092)	1.958(0.625)	2.324(0.466)
EBARS $\gamma = 1$	1000	0.064(0.011)	0.355(0.051)	0.230(0.061)	0.331(0.077)
EBARS $\gamma = 0.5$		0.066(0.016)	0.326(0.056)	0.222(0.053)	0.343(0.078)
EBARS $\gamma = 0$		0.065(0.014)	0.306(0.058)	0.242(0.067)	0.336(0.058)
BARS		0.107(0.027)	0.416(0.094)	0.313(0.074)	1.020(0.510)
TPS		0.057(0.015)	0.319(0.032)	1.205(0.215)	1.379(0.214)

methods is satisfactory and MSE of TPS is roughly the smallest. This indicates that five spline approaches do well in fitting smooth surfaces. However, when the surface is discontinuous, the prediction performance of TPS is worse than free knot splines. For example, the MSE of TPS are much larger than that of EBARS and BARS in Cases 2.3 and 2.4. BARS achieves close results to EBARS except for Case 2.4. As k has to be large enough to fit Case 2.4, the performance of BARS is limited owing to the poor property of BIC in high dimension. Besides, EBARS performs slightly better with low γ than with high γ even in smooth cases, different from curve regression. It seems that surface regression is more likely to be underfitting rather than overfitting.

To graphically illustrate the difference in surface spline regression, we visualize the prediction results with $m = 1000$ by contour maps in Figure 6. Initially, the fitted contours approximately overlap with the ground truth in Cases 2.1 and 2.2, see the top 2 rows. We can see from the (3, 6) and (4, 6) panels that TPS fails to estimate the jump discontinuity in Cases 2.3 and 2.4. Actually, the fitted surfaces by TPS are always smooth regardless of the smoothness of true models. BARS obtains a nice performance in Cases 2.1-2.3, but is trapped in Case 2.4 when the required k is enormous. Conversely, Columns 2 – 4 of Figure 6 show that our EBARS makes precise predictions in all cases successfully.

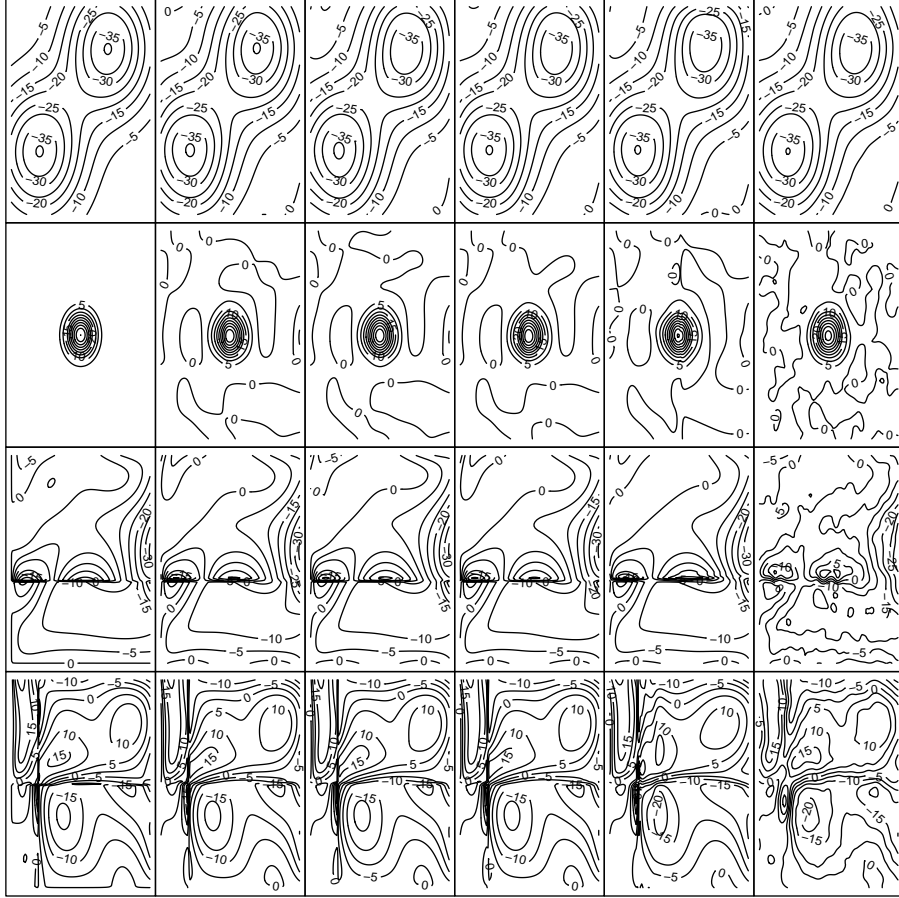


Figure 6: Surface spline regression. It illustrates the prediction results with $m = 1000$ in Cases 2.1 – 2.4 by contours. From left to right, columns are respectively the ground truth, prediction by EBARS with $\gamma = 1, 0.5, 0$, prediction by BARS and prediction by TPS.